Journal of Materials Chemistry A

Accepted Manuscript

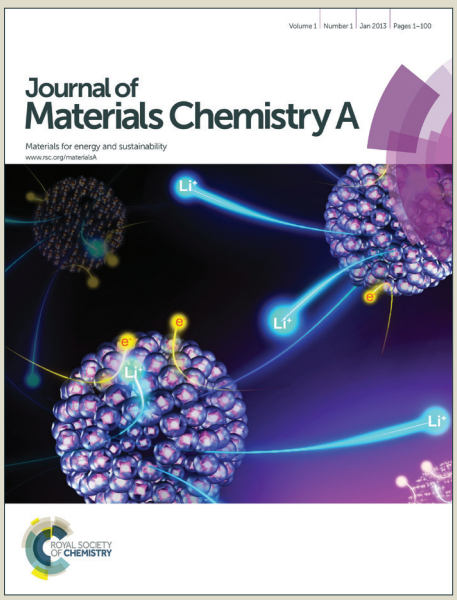

ROYAL SOCIETY OF CHEMISTRY

www.rsc.org/materialsA

Journal name

ARTICLE

A RuO_2 nanoparticle-decorated buckypaper cathode for non-aqueous lithium-oxygen batteries

Received 00th January 20xx,
Accepted 00th January 20xx

DOI: 10.1039/x0xx00000x

www.rsc.org/

P. Tan, W. Shyy, T. S. Zhao*, X. B. Zhu and Z. H. Wei

We report a non-aqueous lithium-oxygen battery with its cathode made of a RuO_2 nanoparticle-decorated buckypaper (weaved with carbon nanotubes). Compared with conventionally slurry-formed cathodes, the present cathode has two striking features: i) no binder is required, avoiding the problems of surface-loss and instability due to the introduction of a polymeric binder; and ii) no additional current collector is needed, increasing the practical specific capacity. The present battery demonstrates a discharge plateau of 2.56 V and a charge plateau of 4.10 V at a current density of 0.4 mA cm^{-2}, with a discharge capacity of 4.72 mAh cm^{-2} (1150 mAh $g_{cathode}^{-1}$). It is also shown that at a fixed capacity of 2.0 mAh cm^{-2}, the energy efficiency of the battery reaches 71.2%, 65.4%, and 58.0% at the current densities of 0.2, 0.4, and 0.8 mA cm^{-2}, respectively. Furthermore, the battery is able to operate for 50 cycles at a fixed capacity of 1.0 mAh cm^{-2}, showing good cycling stability. The results suggest that the RuO_2 nanoparticle-decorated buckypaper cathode offers the promise for a high-practical specific capacity, high-energy efficiency, and stable electrode in non-aqueous lithium-oxygen batteries.

Introduction

Non-aqueous lithium-oxygen batteries are regarded as one of the most promising power sources for electric vehicles and portable devices,[1] mainly due to the high energy density output as a result of two factors.[2-5] First, lithium is the lightest metal and has the highest specific capacity of 3.86×10^3 mAh g^{-1}, corresponding to a specific energy density of 1.14×10^4 Wh kg^{-1} for a theoretical potential of 2.96 V.[6] Second, the cathode active material, oxygen, can be retrieved from ambient air without occupying the battery volume. To make this technology commercially viable, however, a number of technical barriers must be overcome, including low practical discharge capacity, low energy efficiency, and short cycle life.[7-12] A typical non-aqueous lithium-oxygen battery consists of a lithium metal anode, a lithium ion conducting electrolyte, and a porous cathode. During discharge, oxygen is taken from ambient air and reduced at the porous cathode to form the discharge product lithium peroxide (Li_2O_2). Due to its insolubility in the non-aqueous electrolyte, Li_2O_2 grows in the pores of the porous cathode when the capacity is increased, and can eventually block the transport pathways of oxygen, lithium ions, and electrons,[13] terminating the discharge process. During charge, the solid Li_2O_2 discharge product deposited on the cathode must be electrochemically decomposed to lithium and oxygen. A high charge overpotential poses another major challenge,[14-17] which causes a decrease in the energy efficiency and aggravates side reactions,[18] shortening cycle life. Hence, to obtain an optimum battery performance, the cathode must be designed in such a way which can enhance the transport processes as well as the reaction kinetics, while allowing high catalytic activities in charge and discharge processes to lower overpotential.[19]

Tremendous efforts have been made to the development of a suitable cathode for non-aqueous lithium-oxygen batteries. Various kinds of carbon materials with unique morphology and porous structure have been tested, such as carbon powder, nanotubes, and graphene.[20] In addition to the morphology and structure, the surface modifications (e.g. N-doped) of carbon materials have been shown great effects on the battery performance.[21, 22] Besides, different kinds of catalyst materials, especially transition metal oxides and their composites, have been widely investigated.[23-27] Conventionally, the cathode is fabricated by loading the catalyst onto a porous current collector (e.g. carbon paper, [28-30] nickel-based composites [31-34]) through casting of a slurry mixture comprising of the catalyst, conductive matrix (e.g. Ketjen black,[28, 29, 31, 33, 35] Vulcan XC-72 carbon,[30] Super P [32, 34, 36]), and polymeric binder (e.g. polytetrafluoroethylene,[29] polyvinylidene fluoride [28, 30, 33-35]). However, these additives not only complicate fabrication procedures, but also increase the cathode weight. The practical specific capacity is lowed as a result, especially when taking the heavy weight of the current collector into consideration.[37] In our previous works,[9, 10] carbon power and nanotubes with a polymeric binder were used to fabricate the cathode; although no current collectors are required in this type of cathode, the involvement of insulating polymeric binders increases the contact resistance, reducing the effective surface area of the cathode.[38] In addition, the stability of polymeric binders is a critical issue and they pose the problem of decomposing into irreversible side products during battery operation,[39, 40] resulting in poor reversibility. Thus, a cathode that is free of additional current collectors and binders would be ideal in addressing the previously mentioned issues.

Department of Mechanical and Aerospace Engineering, The Hong Kong University of Science and Technology, Clear Water Bay, Kowloon, Hong Kong SAR, China. E-mail: metzhao@ust.hk (T. S. Zhao)

†Electronic Supplementary Information (ESI) available: Fig. S1-S7. See DOI: 10.1039/x0xx00000x

Various types of cathode which are free of additional current collectors and binders have been reported.[41-44] Zhang et al.[42] designed a free-standing MnO_2@carbon paper cathode, with birnessite-type MnO_2 nanosheets grown vertically on the surface of carbon paper and interconnected to form a three-dimensional porous architecture. A battery with this cathode was reported to deliver a capacity of around 140 mAh $g_{cathode}^{-1}$, exhibited over 90 cycles with a capacity of more than 1000 mAh g_{MnO2}^{-1} and a high coulombic efficiency of around 100% in the voltage range of 2.2-4.4 V. Wei et al.[43] fabricated a non-carbon cathode by electrodeposition of an amorphous MnO_2 layer on the surfaces of stainless steel fibers. A battery with this cathode delivered a capacity of 1780 mAh g_{MnO2}^{-1} at 100 mA g_{MnO2}^{-1} and was able to operate for more than 10 cycles with a fixed capacity of 500 mAh g_{MnO2}^{-1}, demonstrating good stability. Kim et al.[44] developed a cathode with Au nanoparticles coated on a nickel nanowire substrate. This cathode showed a high capacity of 921 mAh g_{Au}^{-1} at the current density of 300 mA g_{Au}^{-1}, and exhibited excellent cycle stability with the capacity retention of 98.1% after 100 cycles at 500 mA g_{Au}^{-1}.

In this work, we present a cathode made of a RuO_2 nanoparticle-decorated buckypaper (weaved with carbon nanotubes). Our previous study [10] showed that cathodes formed from interconnected carbon nanotubes had larger pore space than that of the carbon powder-based cathodes, facilitating the transport of species. Buckypaper is a porous structure composed of interpenetrating carbon nanotubes and does not require the employment of binders, preventing surface-loss and instability that would otherwise be introduced with the use of polymeric binder additives. Unlike previously reported buckypaper cathodes which were supported by a metal substrate/current collector,[45-47] no additional current collector is used, increasing the practical specific capacity. RuO_2 has been proven to be an effective catalyst in non-aqueous lithium-air batteries,[29, 48-54] and the cathodes with RuO_2 or RuO_2 decorated supporting materials reported in previous papers were formed through casting of a slurry mixture comprising of the catalysts and binders onto a supporter/current collector.[29, 48-50, 52-54] Here, the cathode was formed by directly decorating RuO_2 nanoparticles onto the surfaces of buckypaper to enhance the catalytic activities. A non-aqueous lithium-oxygen battery was constructed to test the discharge and charge performance of this RuO_2 nanoparticle-decorated buckypaper cathode, and compared to that of a blank buckypaper cathode. The formation and decomposition of the discharge product were detected, and the morphologies of the cathodes after discharge and charge were examined. Moreover, the energy efficiencies of the battery with this RuO_2 nanoparticle-decorated buckypaper cathode at various current densities were studied, as well as the cycling stability.

Experimental

Fabrication of RuO_2/Buckypaper cathode

The buckypaper used in this experiment was composed of multi-walled carbon nanotubes and made via a filtration method (Suzhou Creative Nano-Carbon Co. Ltd., purity: 99.5%, porosity: 75%, specific surface area: 53.8 m^2 g^{-1}, carbon nanotube loading: 4.0 mg cm^{-2}, Fig. S1†). A previous study [45] indicated that the practical specific capacity increases with a decrease in the cathode thickness. However, a thin cathode may require a substrate to ensure a sufficient mechanical strength. The inclusion of the substrate will decrease the practical capacity. In this work, we chose a 60 μm-thick buckypaper as the cathode. As this buckypaper has a sufficient mechanical strength (10 MPa), neither substrate nor current collector is required. To remove the possible residual metal catalysts used in the carbon nanotube fabrication process, the as-received buckypaper was soaked in 10% HCl solution at 40 °C for 6 h and then rinsed with distilled water. After that, the sample was dried under vacuum at 120 °C for 12 h and donated as Buckypaper.

To fabricate the RuO_2 nanoparticle-decorated buckypaper, the as-treated buckypaper was immersed in a 0.01 M $RuCl_3$ solution. A 0.05 M K_2CO_3 aqueous solution was added slowly to the above solution while being stirred until the pH value reached 7, which was monitored by a digital pH meter. Then, the buckypaper was rinsed with distilled water, dried at 80 °C for 8 h and heat treated at 120 °C. The as-prepared sample was donated as RuO_2/Buckypaper. Finally, both the Buckypaper and RuO_2/Buckypaper cathodes for battery test were cut into discs with a diameter of 8 mm.

Material characterization

The cross-section and the surface morphologies of the Buckypaper and RuO_2/Buckypaper cathodes were observed by a scanning electron microscope (SEM, JEOL-6700F) under an acceleration voltage of 5.0 kV. Transmission electron microscopy (TEM) images were obtained by operating a high-resolution JEOL 2010F TEM system with a LaB_6 filament at 200 kV. The samples were dispersed in ethanol, sonicated and dripped onto the holey carbon-coated Cu grids. The BET surface area of the RuO_2/Buckypaper cathode was examined via nitrogen adsorption-desorption. The compositions of the Buckypaper and RuO_2/Buckypaper cathodes were analyzed by a Philips high resolution X-ray diffraction system (XRD, model PW 1825) using a Cu-Kα source operating at 40 keV. The X-ray photoelectron spectroscopy (XPS) characterization was determined by a Physical Electronics PHI 5600 multi-technique system using Al monochromatic X-ray at a power of 350 W. The peak position correction was corrected by referencing the C 1s peak position of carbon (284.8 eV, *PHI Handbook of Photoelectron Spectroscopy*), and shifting all other peaks in the spectrum accordingly. A Fourier-transform infrared (FTIR) test was carried out on a spectrometer (Vertex 70, Bruker) in the frequency range of 400-1000 cm^{-1}. To test the content of RuO_2 in the RuO_2/Buckypaper cathode, thermogravimetric analysis (TGA) was performed on TGA Q5000 (TA instruments) under air atmosphere from 25 °C to 800 °C, heated at a rate of 10 °C per minute.

Electrochemical measurements

The lithium-oxygen battery consists of a lithium metal foil as the anode, a glass-fiber separator (Whatman GF/C), and the cathode as-prepared. The electrolyte was composed of 150 μL 1.0 M lithium Bis(Trifluoromethanesulfonyl)Imide (LiTFSI, Sigma-Aldrich, 99.95%) in tetraethylene glycol dimethyl ether (TEGDME, Sigma-Aldrich, 99%) with the water concentration at less than 5 ppm. To eliminate the influence of moisture on the battery, the cathode electrode and glass-fiber separator were dried in vacuum, and the electrolyte was dried with molecular sieves before use. The battery was assembled

in an argon-filled glove box (Etelux, Lab 2000) at water and oxygen contents below 1 ppm. After assembly, the inlet of the battery was tightly connected to high purity oxygen (≥99.997%, H_2O≤1 ppm, CO_2≤1 ppm) with a constant flow to exhaust the remaining argon. Then, the outlet of the battery was sealed and the battery was exposed to oxygen at a constant pressure of about 1 atm. The galvanostatic discharge and charge tests were conducted on a battery cycling system (Neware, CT-3008W) at a current density of 0.4 mA cm^{-2} (100 mA g^{-1}). To test the energy efficiencies of both Buckypaper and RuO_2/Buckypaper cathodes at different current densities, the battery was discharged and charged at a fixed capacity of 2.0 mAh cm^{-2} with the current density of 0.2, 0.4, and 0.8 mA cm^{-2}, respectively. The cycling stability was tested at the current density of 0.4 mA cm^{-2} with a fixed capacity of 1.0 mAh cm^{-2}, and the cut-off voltage of 2.0 V for discharge and of 4.8 V for charge. All tests were performed at room temperature (25 °C).

The cathode compositions after discharge and charge were analyzed by XRD, FTIR, and XPS. The cathode morphologies after discharge and charge were observed by a SEM. To obtain the cathode after test, the battery was disassembled in the argon glove box, and the cathode was rinsed by pure TEGDME and then dried at room temperature in a vacuum chamber. For all measurements, a home-made gas container filled with argon was used to transfer the cathodes.

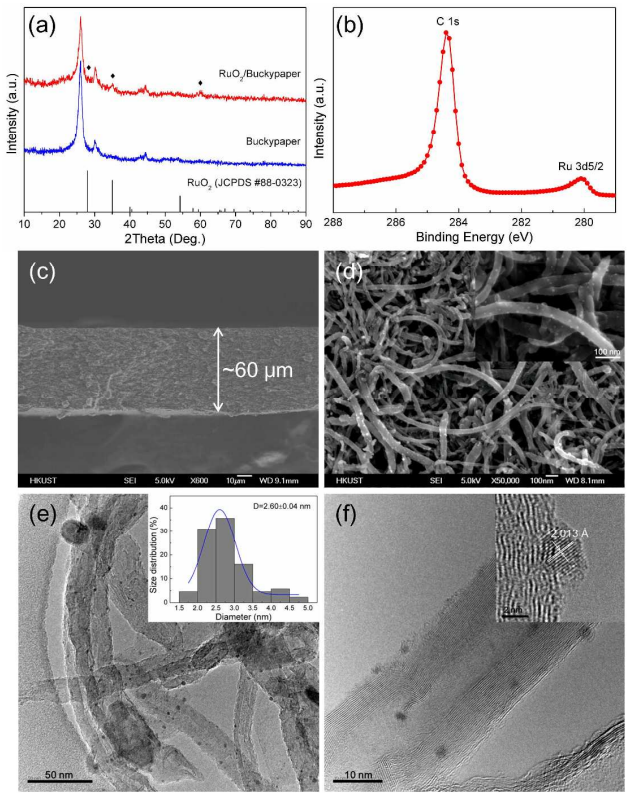

Fig. 1 Characterization of the Buckypaper and RuO_2/Buckypaper cathode: (a) XRD patterns and the reference pattern of RuO_2 according to JCPDS database; (b) XPS spectra of C 1s and Ru 3d; (c) Cross-section of the cathode; (d) The surface morphology (inset: high-resolution SEM image of the RuO_2 nanoparticle-decorated carbon nanotubes); (e) TEM image (inset: the histograms of particle size distribution); and (f) High-resolution TEM image of a multi-walled carbon nanotube with RuO_2 nanoparticles (inset: lattice fringes of RuO_2 nanoparticle).

Results and discussion

Characterization of RuO_2/Buckypaper cathode

The XRD patterns of the Buckypaper and RuO_2/Buckypaper cathodes in the range of 2θ from 10° to 90° are shown in Fig. 1a. For both cathodes, three diffraction peaks are identified as the (002), (100), and (101) peaks of carbon; the peak at 30° may have been caused by residual metal catalysts after acid treatment (~0.36%, Fig. S2a†). For the RuO_2/Buckypaper cathode, three additional diffraction peaks were identified to be the (110), (101), and (002) peaks of RuO_2 (JCPDS # 88-0823), suggesting that RuO_2 was formed. The formation of RuO_2 is further demonstrated by XPS spectra in the range of 279 to 288 eV, as shown in Fig. 1b. The weight content of RuO_2 in the RuO_2/Buckypaper cathode is determined to be ~2.80% through TGA (Fig. S2b†), which is about 0.115 mg cm^{-2}.

The SEM image of the cross-section of the RuO_2/Buckypaper cathode is shown in Fig. 1c. After the decoration of RuO_2 nanoparticles, the RuO_2/Buckypaper cathode maintains a thickness of ~60 μm. The surface morphology of the RuO_2/Buckypaper cathode is shown in Fig. 1d. Carbon nanotubes with diameters of 20 to 60 nm are weaved to form the porous structure, similar to the surface morphology of the Buckypaper cathode (Fig. S3†). In addition, RuO_2 nanoparticles are decorated on the surfaces of carbon nanotubes, as shown in the inset of the high-resolution SEM image. From the TEM image in Fig. 1e, RuO_2 nanoparticles are distributed over the carbon nanotube surface, with an average particle size of 2.60 ± 0.04 nm. The high-resolution TEM image in Fig. 1f shows a multi-walled carbon nanotube decorated with RuO_2 nanoparticles, and clear lattice fringes for RuO_2 are observed in Fig. 1f inset, indicating the crystalline nature of the particles. The regular interplanar spacing of 2.013 Å is ascribed to the (210) plane of RuO_2 (JCPDS # 88-0823). The results demonstrate that RuO_2 nanoparticles are introduced into the buckypaper cathode and decorated on the surface of multi-walled carbon nanotubes.

Discharge and charge performance

The discharge and charge curves of the Buckypaper and the RuO_2/Buckypaper cathode at the current density of 0.4 mA cm^{-2} are present in Fig. 2a. For the Buckypaper cathode, the discharge voltage first decreases to a plateau of 2.53 V, and then gradually decreases with an increase in the discharge capacity. It then drops rapidly to 2.0 V, with a capacity of 4.53 mAh cm^{-2}. On charge, after a short region of about 3.70 V, the voltage increases to a high plateau of 4.50 V, and reaches 4.80 V toward the end of charge. For the RuO_2/Buckypaper cathode, the discharge voltage almost maintains a plateau of about 2.56 V. This higher voltage arises from the high electrocatalytic activity of the RuO_2 nanoparticles for the oxygen reduction reaction.[48] When the voltage drops to 2.0 V, the RuO_2/Buckypaper cathode delivers a capacity of 4.72 mAh cm^{-2}, which is about 4.2% higher than that of the Buckypaper cathode.

Even while taking the additional mass caused by the introduction of RuO_2 nanoparticles (~2.80%) into account, the specific capacity is still slightly larger (1.36%) than that of the Buckypaper cathode. Additionally, considering the total mass, the specific capacity based on the RuO_2/Buckypaper cathode is 1150 mAh $g_{cathode}^{-1}$, a value much higher than that of our previous carbon nanotube-based cathode with the polymeric binder (~730 mAh $g_{cathode}^{-1}$) [9] and the reported MnO_2@carbon paper cathode (~140 mAh $g_{cathode}^{-1}$).[42] On charge, the voltage of the RuO_2/Buckypaper cathode increases to a plateau of about 4.10 V, a reading that is 400 mV lower than that of the Buckypaper cathode, and reaches 4.45 V at the end of charge. Thus, an improved charge performance is obtained using this RuO_2/Buckypaper cathode. To study the effect of RuO_2 loading on the electrochemical performance, we prepared another RuO_2/Buckypaper cathode with the RuO_2 loading of ~7.62% (Fig. S2c†, 0.330 mg cm^{-2}). It is seen that the discharge voltage plateau has a little increase of ~10 mV, and the charge voltage plateau remarkably decreases to 3.94 V (Fig. S4†). However, the discharge capacity decreases to 3.91 mAh cm^{-2} (900 mAh $g_{cathode}^{-1}$), which is smaller than that of the Buckypaper cathode. Similar results have been reported by Yilmaz et al, in which the RuO_2/CNT cathode with 32 wt % RuO_2 has a lower charge voltage but a decreased capacity than that of a CNT cathode.[48] The decreased discharge capacity may be attributed to the decrease in the specific surface areas [49] (Fig. S5†) and the changes in the discharge product morphology.[51] To avoid the sacrifice of the capacity, in our following study, we focused on the RuO_2/Buckypaper cathode with the RuO_2 loading of ~2.80%.

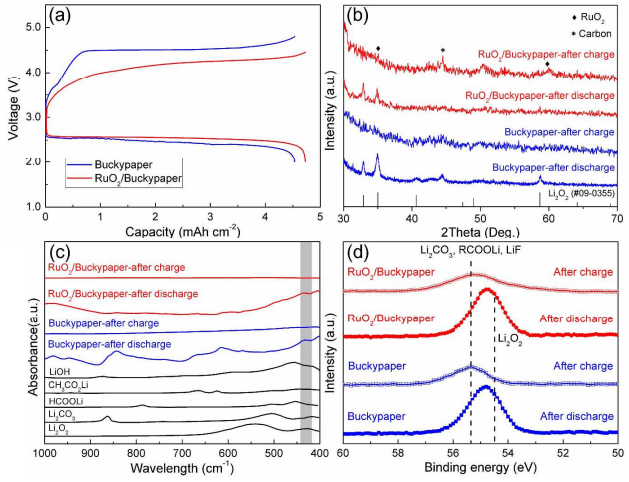

Fig. 2 Discharge and charge characterization of the Buckypaper and RuO_2/Buckypaper cathode: (a) Voltage curves at the current density of 0.4 mA cm^{-2}; (b) XRD patterns of the cathodes after discharge and charge; (c) FTIR spectra of the cathodes after discharge and charge; and (d) Li 1s spectra of the cathodes after discharge and charge.

To study the compositions of the Buckypaper and RuO_2/Buckypaper cathodes after discharge and charge, XRD, FTIR, and XPS were employed, and the results are present in Fig. 2b-2d, respectively. Fig. 2b shows the XRD patterns of both cathodes. For the Buckypaper cathode, after discharge the peaks are identified as the (100), (101), (102), and (110) peaks of Li_2O_2 (JCPDS #09-0355), suggesting that the main discharge product is Li_2O_2. After charge, these peaks disappear, indicating the decomposition of Li_2O_2. For the RuO_2/Buckypaper cathode, after discharge the (100), (101), and (110) peaks of Li_2O_2 are detected, and the (002) peak related to RuO_2 disappears, suggesting that Li_2O_2 covers the surface of RuO_2 nanoparticles (Fig. S6†). After charge, the peaks correspond to Li_2O_2 disappear, while the peaks correspond to carbon and RuO_2 re-appear, demonstrating that the discharge product is removed from the surfaces of carbon nanotubes and RuO_2 nanoparticles. FTIR spectra for the discharged and charged Buckypaper and RuO_2/Buckypaper cathodes are present in Fig. 2c. The absorbance peak at around 430 cm^{-1} (marked as the shaded area) is derived from Li_2O_2 in the discharged Buckypaper and RuO_2/Buckypaper cathodes, and its disappearance in the charged cathodes indicates the decomposition of Li_2O_2 in the following charge process. Fig. 2d compares the Li 1s XPS spectra of the discharged and charged cathodes. The Li 1s region for the Buckypaper and RuO_2/Buckypaper cathode after discharge includes contribution from the underlying Li_2O_2 (Li 1s: 54.5 eV) [55] and surface lithium carbonate species (Li 1s: 55.3 eV) [55] formed by the reaction between electrolyte and Li_2O_2. Upon charge, for both Buckypaper and RuO_2/Buckypaper cathodes, the Li 1s peak corresponding to Li_2O_2 disappears, suggesting the decomposition of Li_2O_2.[56] On the basis of the above XRD, FTIR, and XPS results, it is demonstrated that for both Buckypaper and RuO_2/Buckypaper cathodes, Li_2O_2, as the major discharge product, is reversibly formed in the discharge process and is decomposed in the following charge process.

To provide insight for how a RuO_2/Buckypaper cathode leads to a lower charge voltage than that of the Buckypaper cathode, we examined the morphologies of both cathodes after discharge. For the Buckypaper cathode, at the side facing oxygen the surface is fully covered by the Li_2O_2 particles with a disc-like morphology (Fig. 3a1), congruent with previous reports;[56-58] at the side facing the separator (Fig. 3a2), however, the carbon nanotube surfaces are covered with a film-like discharge product with remaining open pores. We explain that the oxygen concentration in the cathode decreases from the oxygen side to the separator side during discharge, and a higher oxygen concentration results in a higher reaction rate. Hence, the fraction of the solid product is larger at the oxygen side, which decreases toward the separator side (Fig. S7a†). The large-sized particles at the oxygen side eventually occupies the pores, which act as further blockages to the oxygen transport pathway and lead to low utilization of the inner region near the separator. In the charge process, the decomposition of film-like discharge product may occur initially due to enlarged contact areas within the electrolyte and carbon nanotube surfaces, resulting in the lower charge voltage region,[15] followed by the decomposition of large-sized particles with a higher charge voltage plateau,[15] which is consistent with the charge curve in Fig. 2a. For the RuO_2/Buckypaper cathode, as shown in Fig. 3b1 and 3b2, both sides facing the oxygen and separator present a similar morphology, with a film-like discharge product covering the surface. First-principle calculations showed that Li_2O_2 is likely to wet the RuO_2 surfaces and grow into thin films rather than particles,[51] and

previous experiments demonstrated that RuO_2 nanoparticles contribute to the formation of poorly crystalline Li_2O_2 that is coated over the carbon nanotubes with a large contact area.[48] Therefore, the change in morphology of the discharge product is caused by the introduction of RuO_2 nanoparticles onto the carbon nanotube surface. During discharge, the film-like Li_2O_2 morphology facilitates the oxygen transport, which helps to utilize the whole cathode (Fig. S7b†). In the charge process, the increased contact area of the discharge product associated with possible increased electrical conductivity due to the poorly crystalline Li_2O_2 [48] results in the lower charge voltage, as shown in Fig. 1a. It is also worth noting although the charge performance improved with the addition of RuO_2 nanoparticles, the film-like product morphology may lead to a lower discharge capacity than that of large-sized product particles,[59-61] which may be used to explain the decreased capacity in Yilmaz's work [48] and the decrease in capacity with an increase in the RuO_2 loading in our experiment (Fig. S4†). After charge, as shown in Fig. 3a3 and 3b3, the surfaces of Buckypaper and RuO_2/Buckypaper cathodes recovered to their pristine states, indicating that the discharge product had indeed decomposed, consistent with the results from XRD, FTIR and XPS.

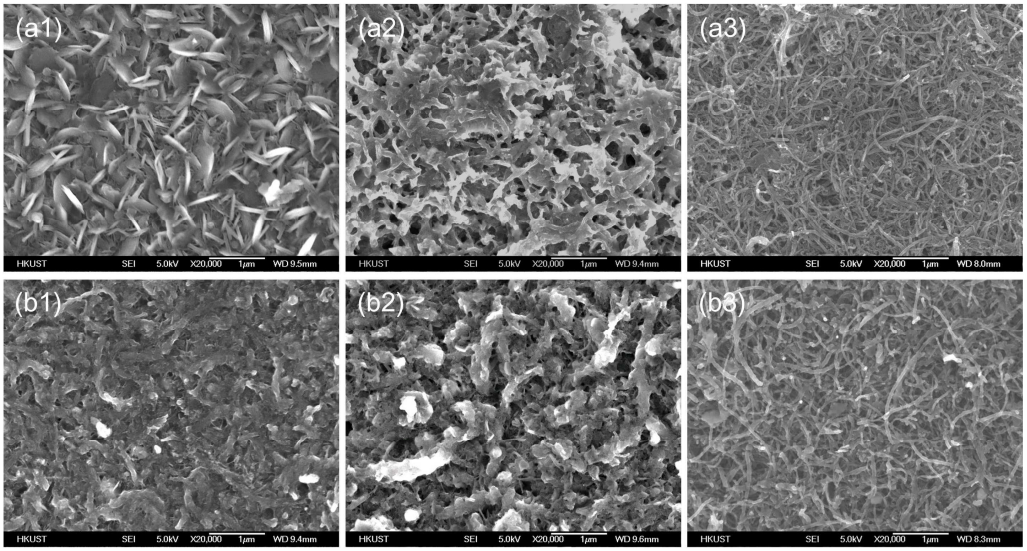

Fig. 3 SEM image of the (a) Buckypaper and (b) RuO_2/Buckypaper cathode after discharge (1: oxygen-side, 2: separator-side) and after charge (3) at the current density of 0.4 mA cm^{-2}.

Energy efficiency

The energy efficiencies of the battery with the Buckypaper and the RuO_2/Buckypaper cathode at various current densities were studied with a fixed capacity of 2.0 mAh cm^{-2}, and the results are shown in Fig. 4. At the current density of 0.2 mA cm^{-2}, as shown in Fig. 4a, the discharge and charge voltage plateau of the Buckypaper cathode is about 2.60 V and 4.36 V, respectively. For the RuO_2/Buckypaper cathode, the discharge voltage plateau is about 2.65 V, with an increase of 50 mV; while the charge voltage plateau only reaches 3.76 V, with a remarkable decrease of 600 mV. When the current density increases to 0.4 mA cm^{-2}, as shown in Fig. 4b, the discharge and charge voltage plateau of the Buckypaper cathode is about 2.53 V and 4.50 V, respectively. For the RuO_2/Buckypaper cathode, the discharge and charge voltage plateau is about 2.57 V and 3.95 V, respectively. With an increase in the current density to 0.8 mA cm^{-2}, as shown in Fig. 4c, the discharge voltage plateau of the Buckypaper and RuO_2/Buckypaper cathode is about 2.33 V and 2.36 V, respectively; and the charge voltage plateau is about 4.68 V and 4.20 V, respectively. Hence, the RuO_2/Buckypaper cathode leads to an increase in the discharge voltage and a large decrease in the charge voltage at various current densities, resulting in a higher energy efficiency than that of the Buckypaper cathode. As shown in Fig. 4d, when the current density increases from 0.2 to 0.4 mA cm^{-2}, the energy efficiency of the RuO_2/Buckypaper cathode decreases from 71.2% to 65.4%, higher than that of the Buckypaper cathode which decreases from 61.0% to 57.0%. Even at a large current density of 0.8 mA cm^{-2}, the energy efficiency of the RuO_2/Buckypaper cathode is still as high as 58.0%, showing a remarkable improvement than that of the Buckypaper cathode.

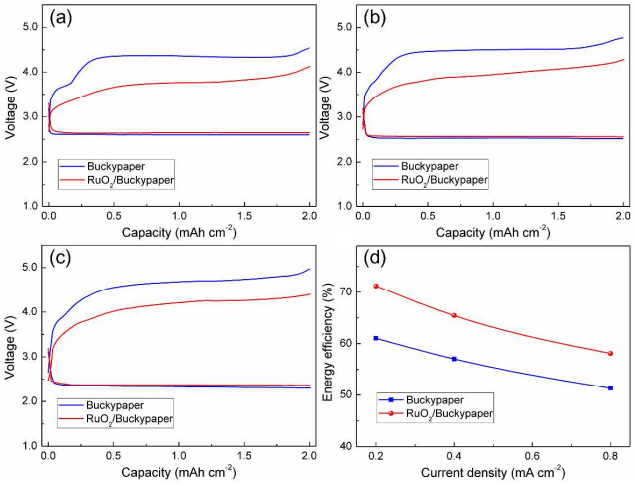

Fig. 4 Discharge and charge curves of the Buckypaper and RuO_2/Buckypaper cathode at the current density of (a) 0.2 mA cm^{-2}, (b) 0.4 mA cm^{-2}, and (c) 0.8 mA cm^{-2} with a fixed capacity of 2.0 mAh cm^{-2}, respectively; (d) Comparison of the energy efficiency at various current densities.

Cycling stability

The cycling stability of the battery with the RuO_2/Buckypaper cathode was tested at the current density of 0.4 mA cm^{-2} with a fixed capacity of 1.0 mAh cm^{-2}, and compared with that of the battery with the Buckypaper cathode. As shown in Fig. 5a, the discharge voltage plateau of the Buckypaper cathode is about 2.53 V, and continues to decrease with cycling. On the contrary, the charge voltage plateau is about 4.40 V, and increases with cycling. The high charge voltage would cause the decompositions of the electrolyte and the carbon cathode to form the irreversible side products.[18] The charge voltage reaches 4.80 V at the 21st cycle before being fully charged, remaining some undecomposed discharge product Li_2O_2. The accumulation of side products and undecomposed Li_2O_2 in the Buckypaper cathode decreases the reaction sites and increases the transport resistances, and eventually leads to the capacity decay at the 30th cycle. For the battery with the RuO_2/Buckypaper cathode, as shown in Fig. 5b, the discharge voltage plateau for the first cycle is about 2.56 V, while the charge voltage plateau is about 3.94 V, which is remarkably 460 mV lower than that of the Buckypaper cathode. With an increase of the cycle number, the discharge voltage gradually decreases, and the charge voltage increases, which may be attributed to the accumulation of side products caused by the decomposition of electrolyte [62] (as shown in XPS results in Fig. 2d) and the passivation of the lithium anode due to oxygen crossover.[63, 64] Even at the 50th cycle, the discharge voltage plateau remains at 2.31 V, and the terminal charge voltage at 4.75 V. Thus, the battery with the RuO_2/Buckypaper cathode can maintain its discharge capacity and coulombic efficiency for 50 cycles without signs of degradation, as shown in Fig. 5c and 5d, respectively, demonstrating good cycling stability.

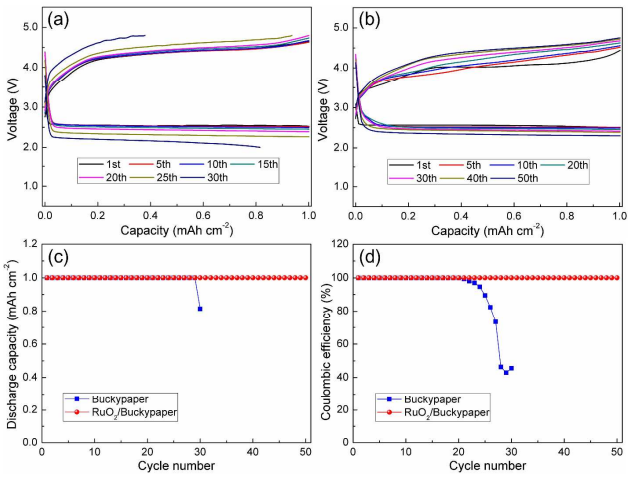

Fig. 5 Cycling stability of the Buckypaper and RuO_2/Buckypaper cathode: Discharge/charge curves of a lithium-oxygen battery using (a) Buckypaper and (b) RuO_2/Buckypaper cathode at 0.4 mA cm^{-2} with a fixed capacity of 1.0 mAh cm^{-2}; (c) Discharge capacity and (d) Coulombic efficiency as a function of cycle number.

Conclusions

In this work, we have created a non-aqueous lithium-oxygen battery with its cathode made of a RuO_2 nanoparticle-decorated buckypaper (weaved with carbon nanotubes). Compared with conventionally slurry-formed cathodes, the present cathode is free of binders, avoiding surface-loss and instability problems introduced from polymeric binders. In addition, the cathode does not need an additional current collector, leading to an increase in the practical specific capacity. The present battery demonstrates a discharge plateau of 2.56 V and a charge plateau of 4.10 V at a current density of 0.4 mA cm^{-2}, with a discharge capacity of 4.72 mAh cm^{-2} (1150 mAh $g_{cathode}^{-1}$). The reversible formation and decomposition of Li_2O_2 as the major product in the discharge and charge processes were demonstrated by XRD, FTIR, and XPS. The SEM images showed that for the blank buckypaper cathode, the discharge product on the oxygen and separator sides presented different morphologies, with large disc-like morphology at the oxygen-side and film-like morphology at the separator-side. However, for the RuO_2 nanoparticle-decorated buckypaper cathode, the product on both sides showed similar film-like morphologies. Hence, the decreased charge voltage may be derived from a change in the product morphology and possible poor crystalline discharge product due to the contribution of RuO_2 nanoparticles. It is also shown that at a fixed capacity of 2.0 mAh cm^{-2}, the energy efficiency of the battery reaches 71.2%, 65.4%, and 58.0% at the current densities of 0.2, 0.4, and 0.8 mA cm^{-2}, respectively. Furthermore, the present battery is able to operate for 50 cycles at a fixed capacity of 1.0 mAh cm^{-2}, showing good cycling stability. The results demonstrate that the RuO_2 nanoparticle-decorated buckypaper cathode does not require additional current collectors and polymeric binders, hence offers the promise for a high-practical specific capacity, high-energy efficiency, and stable electrode in non-aqueous lithium-oxygen batteries.

Acknowledgements

The work described in this paper was fully supported by a grant from the Research Grants Council of the Hong Kong Special Administrative Region, China (project no. 622712).

Notes and references

1 G. Girishkumar, B. McCloskey, A. C. Luntz, S. Swanson and W. Wilcke, *Journal of Physical Chemistry Letters,* 2010, **1**, 2193-2203.
2 J. P. Zheng, R. Y. Liang, M. Hendrickson and E. J. Plichta, *J. Electrochem. Soc.,* 2008, **155**, A432-A437.
3 J. Lee, S. Tai Kim, R. Cao, N. Choi, M. Liu, K. T. Lee and J. Cho, *Advanced Energy Materials,* 2011, **1**, 34-50.
4 P. G. Bruce, S. A. Freunberger, L. J. Hardwick and J. Tarascon, *Nature Materials,* 2012, **11**, 19-29.
5 P. Tan, Z. Wei, W. Shyy and T. S. Zhao, *Appl. Energy,* 2013, **109**, 275-282.

6 I. Kowalczk, J. Read and M. Salomon, *Pure and Applied Chemistry,* 2007, **79**, 851-860.
7 H. Wang and K. Xie, *Electrochim. Acta,* 2012, **64**, 29-34.
8 C. N. Chervin, M. J. Wattendorf, J. W. Long, N. W. Kucko and D. R. Rolison, *J. Electrochem. Soc.,* 2013, **160**, A1510-A1516.
9 P. Tan, W. Shyy, L. An, Z. H. Wei and T. S. Zhao, *Electrochemistry Communications,* 2014, **46**, 111-114.
10 P. Tan, W. Shyy, Z. H. Wei, L. An and T. S. Zhao, *Electrochim. Acta,* 2014, **147**, 1-8.
11 Y. Lu, B. M. Gallant, D. G. Kwabi, J. R. Harding, R. R. Mitchell, M. S. Whittingham and Y. Shao-Horn, *Energy Environ. Sci.,* 2013, **6**, 750-768.
12 F. Li, T. Zhang and H. Zhou, *Energy Environ. Sci.,* 2013, **6**, 1125-1141.
13 V. Viswanathan, K. S. Thygesen, J. S. Hummelshoj, J. K. Norskov, G. Girishkumar, B. D. McCloskey and A. C. Luntz, *J. Chem. Phys.,* 2011, **135**, 214704.
14 B. M. Gallant, D. G. Kwabi, R. R. Mitchell, J. Zhou, C. V. Thompson and Y. Shao-Horn, *Energy Environ. Sci.,* 2013, **6**, 2518-2528.
15 Y. Hu, X. Han, F. Cheng, Q. Zhao, Z. Hu and J. Chen, *Nanoscale,* 2014, **6**, 177-180.
16 P. Tan, W. Shyy, T. S. Zhao, Z. H. Wei and L. An, *J. Power Sources,* 2015, **278**, 133-140.
17 P. Tan, W. Shyy and T. Zhao, *Science Bulletin,* 2015, **60**, 975-976.
18 M. M. Ottakam Thotiyl, S. A. Freunberger, Z. Peng and P. G. Bruce, *J. Am. Chem. Soc.,* 2013, **135**, 494-500.
19 Y. Lu, B. M. Gallant, D. G. Kwabi, J. R. Harding, R. R. Mitchell, M. S. Whittingham and Y. Shao-Horn, *Energy Environ. Sci.,* 2013, **6**, 750-768.
20 Z. Zhang, Q. Zhang, Y. Chen, J. Bao, X. Zhou, Z. Xie, J. Wei and Z. Zhou, *Angewandte Chemie International Edition,* 2015, **54**, 6550-6553.
21 Y. Jing and Z. Zhou, *ACS Catal.,* 2015, **5**, 4309-4317.
22 Z. Zhang, J. Bao, C. He, Y. Chen, J. Wei and Z. Zhou, *Advanced Functional Materials,* 2014, **24**, 6826-6833.
23 W. Yang, J. Salim, S. Li, C. Sun, L. Chen, J. B. Goodenough and Y. Kim, *Journal of Materials Chemistry,* 2012, **22**, 18902-18907.
24 W. Yang, J. Salim, C. Ma, Z. Ma, C. Sun, J. Li, L. Chen and Y. Kim, *Electrochemistry Communications,* 2013, **28**, 13-16.
25 C. Sun, F. Li, C. Ma, Y. Wang, Y. Ren, W. Yang, Z. Ma, J. Li, Y. Chen, Y. Kim and L. Chen, *J. Mater. Chem. A,* 2014, **2**, 7188-7196.
26 Z. Zhang, Y. Chen, J. Bao, Z. Xie, J. Wei and Z. Zhou, *Particle & Particle Systems Characterization,* 2015, **32**, 680-685.
27 Y. Chen, Q. Zhang, Z. Zhang, X. Zhou, Y. Zhong, M. Yang, Z. Xie, J. Wei and Z. Zhou, *J. Mater. Chem. A,* 2015, *DOI: 10.1039/C5TA02990B*.
28 R. Choi, J. Jung, G. Kim, K. Song, Y. Kim, S. C. Jung, Y. Han, H. Song and Y. Kang, *Energy Environ. Sci.,* 2014, **7**, 1362-1368.
29 K. Guo, Y. Li, J. Yang, Z. Zou, X. Xue, X. Li and H. Yang, *J. Mater. Chem. A,* 2014, **2,** 1509-1514.
30 J. Zhang, L. Wang, L. Xu, X. Ge, X. Zhao, M. Lai, Z. Liu and W. Chen, *Nanoscale,* 2015, **7,** 720-726.
31 J. Xu, Z. Wang, D. Xu, F. Meng and X. Zhang, *Energy Environ. Sci.,* 2014, **7,** 2213-2219.
32 C. Shang, S. Dong, P. Hu, J. Guan, D. Xiao, X. Chen, L. Zhang, L. Gu, G. Cui and L. Chen, *Sci. Rep.,* 2015, **5,** 8355.
33 F. Wang, Z. Wen, C. Shen, K. Rui, X. Wu and C. Chen, *J. Mater. Chem. A,* 2015, **3**, 7600-7606 .
34 S. Peng, Y. Hu, L. Li, X. Han, F. Cheng, M. Srinivasan, Q. Yan, S. Ramakrishna and J. Chen, *Nano Energy,* 2015.
35 S. Chen, G. Liu, H. Yadegari, H. Wang and S. Z. Qiao, *J. Mater. Chem. A,* 2015, **3**, 2559-2563.
36 J. Liu, R. Younesi, T. Gustafsson, K. Edström and J. Zhu, *Nano Energy,* 2014, **10**, 19-27.
37 J. Lu, L. Li, J. Park, Y. Sun, F. Wu and K. Amine, *Chem. Rev.,* 2014, **114**, 5611-5640.
38 B. Li, X. Ge, F. W. T. Goh, T. S. A. Hor, D. Geng, G. Du, Z. Liu, J. Zhang, X. Liu and Y. Zong, *Nanoscale,* 2015, **7**, 1830-1838.
39 R. Black, S. H. Oh, J. Lee, T. Yim, B. Adams and L. F. Nazar, *J. Am. Chem. Soc.,* 2012, **134**, 2902-2905.
40 J. Hojberg, B. D. McCloskey, J. Hjelm, T. Vegge, K. Johansen, P. Norby and A. C. Luntz, *ACS Appl. Mater. Interfaces,* 2015, **7**, 4039-4047.
41 Y. Cui, Z. Wen and Y. Liu, *Energy Environ. Sci.,* 2011, **4**, 4727-4734.
42 L. Zhang, F. Zhang, G. Huang, J. Wang, X. Du, Y. Qin and L. Wang, *J. Power Sources,* 2014, **261**, 311-316.
43 Z. H. Wei, P. Tan, L. An and T. S. Zhao, *Appl. Energy,* 2014, **130**, 134-138.
44 S. T. Kim, N. Choi, S. Park and J. Cho, *Advanced Energy Materials,* 2014, **5**, 1401030.
45 G. Q. Zhang, J. P. Zheng, R. Liang, C. Zhang, B. Wang, M. Hendrickson and E. J. Plichta, *J. Electrochem. Soc.,* 2010, **157**, A953-A956.
46 Y. Chen, F. Li, D. Tang, Z. Jian, C. Liu, D. Golberg, A. Yamada and H. Zhou, *J. Mater. Chem. A,* 2013, **1**, 13076-13081.
47 D. S. Kim and Y. J. Park, *Solid State Ionics,* 2014, **268**, Part B, 216-221.
48 E. Yilmaz, C. Yogi, K. Yamanaka, T. Ohta and H. R. Byon, *Nano Letters,* 2013, **13**, 4679-4684.
49 Z. Jian, P. Liu, F. Li, P. He, X. Guo, M. Chen and H. Zhou, *Angewandte Chemie-International Edition,* 2014, **53**, 442-446.
50 P. Bhattacharya, E. N. Nasybulin, M. H. Engelhard, L. Kovarik, M. E. Bowden, X. S. Li, D. J. Gaspar, W. Xu and J. Zhang, *Advanced Functional Materials,* 2014, **24**, 7510-7519.
51 W. T. Geng and T. Ohno, *J. Phys. Chem. C, 2015,* **119**, 1024-1031.
52 H. Jang, A. Zahoor, J. S. Jeon, P. Kim, Y. S. Lee and K. S. Nahm, *Journal of the Electrochemical Society,* 2015, **162**, A300-A307.
53 Z. Guo, D. Zhou, H. Liu, X. Dong, S. Yuan, A. Yu, Y. Wang and Y. Xia, *J. Power Sources,* 2015, **276**, 181-188.
54 F. Li, D. Tang, T. Zhang, K. Liao, P. He, D. Golberg, A. Yamada and H. Zhou, *Advanced Energy Materials,* 2015, 1500249.
55 Y. Lu, E. J. Crumlin, G. M. Veith, J. R. Harding, E. Mutoro, L. Baggetto, N. J. Dudney, Z. Liu and Y. Shao-Horn, *Scientific Reports,* 2012, **2**, 715.
56 L. Nazar, D. Kundu, R. Black and E. Jamstorp, *Energy Environ. Sci.,* 2014, **8**, 1292-1298.
57 R. R. Mitchell, B. M. Gallant, Y. Shao-Horn and C. V. Thompson, *Journal of Physical Chemistry Letters,* 2013, **4**, 1060-1064.
58 S. Huang, W. Fan, X. Guo, F. Meng and X. Liu, *ACS Appl. Mater. Interfaces,* 2014, **6**, 21567-75.

59 L. Johnson, C. Li, Z. Liu, Y. Chen, S. A. Freunberger, P. C. Ashok, B. B. Praveen, K. Dholakia, J. Tarascon and P. G. Bruce, *Nat Chem,* 2014, **6**, 1091-1099.
60 N. B. Aetukuri, B. D. McCloskey, J. M. Garcia, L. E. Krupp, V. Viswanathan and A. C. Luntz, *Nat Chem,* 2015, **7**, 50-56.
61 A. Khetan, A. Luntz and V. Viswanathan, *Journal of Physical Chemistry Letters,* 2015, **6**, 1254-1259.
62 H. Lim, K. Park, H. Gwon, J. Hong, H. Kim and K. Kang, *Chemical Communications,* 2012, **48**, 8374-8376.
63 J. Shui, J. S. Okasinski, P. Kenesei, H. A. Dobbs, D. Zhao, J. D. Almer and D. Liu, *Nature Communications,* 2013, **4**, 2255.
64 R. S. Assary, J. Lu, P. Du, X. Luo, X. Zhang, Y. Ren, L. A. Curtiss and K. Amine, *ChemSusChem,* 2013, **6**, 51-55.

Graphic abstract

A RuO_2 nanoparticle-decorated buckypaper cathode does not require additional current collectors and polymeric binders, offers the promise for a high-practical specific capacity, high-energy efficiency, and stable electrode in non-aqueous lithium-air batteries.